Structure, Vol. 13, 1487–1498, October, 2005, ©2005 Elsevier Ltd All rights reserved. DOI 10.1016/j.str.2005.06.015

Functional Plasticity in the Substrate Binding Site of β-Secretase

Alemayehu A. Gorfe* and Amedeo Caflisch*
Department of Biochemistry
University of Zurich
Winterthurerstrasse 190
CH-8057 Zurich
Switzerland

Summary

The aspartic protease β-secretase (BACE) cleaves the amyloid precursor protein into a 42 residue β-peptide, which is the principal biochemical marker of Alzheimer's disease. Multiple explicit-water molecular dynamics simulations of the apo and inhibitor bound structures of BACE indicate that both open- and closed-flap conformations are accessible at room temperature and should be taken into account for inhibitor design. Correlated motion is observed within each of the two lobes of BACE, as well as for the interfacial region. A self-inhibited conformation with the side chain of Tyr71 occupying the S_1 pocket is present in some of the unbound simulations. The reversible loss of the side chain hydrogen bond between the catalytic Asp32 and Ser35, due to the concomitant reorientation of the Ser35 hydroxyl group and a water molecule conserved in pepsin-like enzymes, provides further evidence for the suggestion that Ser35 assists in proton acceptance and release by Asp32 during catalysis.

Introduction

Human β-secretase (BACE, also called memapsin-2 or ASP-2) is a membrane-associated, pepsin-like aspartic protease that cleaves the amyloid precursor protein to generate the 42 residue amyloid-β peptide (Aβ). Since Aβ is the principal biochemical marker of Alzheimer's disease, BACE is a pharmacologically important enzyme target (Ghosh et al., 2002; Roggo, 2002; Citron, 2004; Cumming et al., 2004). Unlike retroviral aspartic proteases, whose active enzyme is a dimer of two identical subunits (Wlodawer et al., 1989; Navia et al., 1989), eukaryotic aspartic proteases are characterized by a bilobal structure made up of two segments of a single polypeptide chain. Two adjacent aspartates, one from each lobe (monomer in retroviral proteases), constitute the catalytic dyad. The structures of the free and inhibitor bound pepsin-like protease are similar, but they often differ in the conformation of a β hairpin, or flap, capping the central part of the substrate binding site. In the presence of inhibitor, the flap is generally in a closed conformation and tightly covers the inhibitor. The open conformation of the flap allows entrance of the substrate and presumably removal of hydrolytic products during the catalytic turnover (Andreeva and Rumsh, 2001). However, the extent of flap opening varies significantly among structures and among different enzymes. In fact, in the majority of the available apo structures of eukaryotic aspartic proteases (e.g., human cathepsin D, PDB code [Berman et al., 2000] 1lya; renin, 2ren; pepsin, 1psn; porcine pepsin, 4pep; saccharopepsin, 1fmu; and endothiapepsin, 2ape), the flap is either in the closed conformation or the opening is not sufficiently wide to allow substrate entrance and product exit. In contrast, the opening can be as large as 7 Å at the tip of the two flaps of the human immunodeficiency virus type 1 (HIV-1) protease in the absence of inhibitor (Wlodawer and Gustchina, 2000).

Tang and coworkers have solved the structure of BACE in complex with the peptidic inhibitors OM99-2 and OM00-3 at a resolution of 1.9 Å and 2.1 Å, respectively (Hong et al., 2000, 2002). BACE shares common structural motifs with other pepsin-like aspartic proteases, but contains several flexible insertion segments (Figure 1A). Because of the strong pharmaceutical interest in designing compounds that block the action of BACE, efforts in structure-based drug design have produced several structures of BACE complexed with molecules of varying sizes and chemical composition (Coburn et al., 2004; Patel et al., 2004; Stachel et al., 2004; Turner et al., 2005; Ghosh et al., 2005). In these structures, the flap (residues 67–77) adopts the closed conformation, and several of its residues directly interact with the bound inhibitor.

Open-flap conformations in free BACE were observed in two X-ray structures recently resolved to 2 Å (APO1 from hereon) (Hong and Tang, 2004) and 1.75 Å (APO2) (Patel et al., 2004). Despite the overall similarity between the free and inhibitor bound structures (the backbone root mean square deviation [rmsd] is 0.6–0.7 Å [Hong and Tang, 2004; Patel et al., 2004]), the tip of the flap has a Cα displacement with respect to the OM99-2 structure of 4.5 Å and 7 Å in APO1 and APO2, respectively. Furthermore, the side chain of the completely conserved residue Tyr71 (Tyr75 in pepsin numbering) near the flap tip has an unusual orientation in APO1 and acts as a donor for a hydrogen bond with the carbonyl oxygen of Lys107 outside the substrate binding site. Usually, Tyr71 is involved in a chain of hydrogen bonds with several residues in the substrate binding pocket (Andreeva and Rumsh, 2001), thus fixing the flap in a closed conformation upon inhibitor or substrate binding. Unusual Tyr71 orientations were previously observed in the uncomplexed chymosin (Gilliland et al., 1990) and the trigonal crystal form of saccharopepsin (Gustchina et al., 2002), where the Tyr71 side chain occupies the S_1 pocket in a self-inhibitory mode (Andreeva et al., 1992). Tyr71 was also suggested to play a role in the capture and cleavage of substrates (Tang and Koelsch, 1995). Another interesting difference between the two apo structures of BACE involves a short loop (residues 9–14, also called the "10s loop" [Patel et al., 2004]) located between two strands at the base of the S_3 subpocket (see Figure 1B for subsite locations). This loop is in a closed conformation in

*Correspondence: abebe@bioc.unizh.ch (A.A.G.); caflisch@bioc.unizh.ch (A.C.)

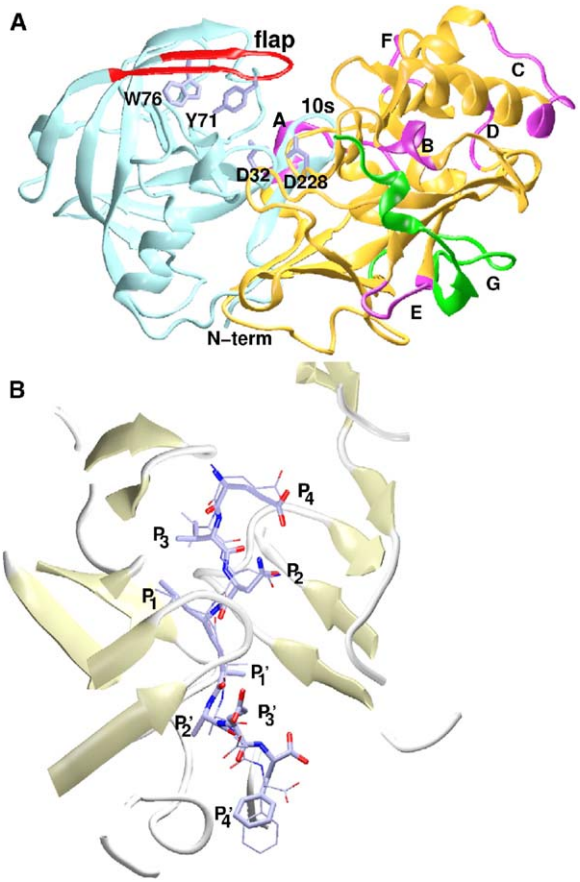

Figure 1. Structure of BACE

(A) Ribbon diagram of BACE in complex with the inhibitor OM99-2 (PDB code 1fkn) (Hong et al., 2000), which was removed for clarity. The N-terminal lobe (residues 1–150) and the C-terminal lobe (residues 151–385) are cyan and orange, respectively. The flap (residues 67–77) is in red; insertion segments (Hong et al., 2000) A–F and G are in purple and green, respectively. The catalytic aspartates and the two flap residues involved in a hydrogen bond are labeled and shown in sticks.

(B) The BACE binding site with the inhibitor OM99-2. The coordinates of the inhibitor from the crystal structure and after 20 ns of the om99-b simulation are shown with thick and thin lines, respectively. It is interesting to note that the P_3'-P_4' C-terminal residues (Glu-Phe) show the highest displacement, which is consistent with their high B factors (Hong et al., 2000).

APO1, while it adopts a significantly more open conformation (a maximal C_α displacement of 4.5 Å from the OM99-2 structure) in APO2. Note that the S_3 subpocket is more open in BACE (and in renin, a pepsin-like aspartic protease involved in the regulation of blood pressure) than in other single-chain aspartic proteases (Patel et al., 2004). The discovery of potent renin inhibitors that exploit this region (Wood et al., 2003; Rahuel et al., 2000) underscores the importance of investigating structural plasticity in protease binding sites.

The role of individual amino acids and water molecules neighboring the catalytic aspartates (Asp32/Asp228 in BACE) of pepsin-like enzymes is not clearly understood. A study based on the analysis of 82 crystal structures suggested that the different hydrogen bonding patterns of the two active aspartates with the adjacent residues are responsible for their optimal activity at low pH (Andreeva and Rumsh, 2001). Furthermore, two completely conserved water molecules were observed. The first water is located between the carboxyl groups of the catalytic aspartates and was proposed to act as a nucleophile. The second conserved water molecule is involved in a hydrogen bond with the hydroxyl group of Tyr71, and this bond bridges the chain of hydrogen bonded residues between the flap and the catalytic aspartates upon ligand binding (Andreeva and Rumsh, 2001; Prasad and Suguna, 2002).

Receptor rearrangement upon ligand binding as the main complicating factor in structure-based ligand design is a widely appreciated problem (Teague, 2003; Cavasotto and Abagyan, 2004). Detailed structural analysis and generation of a statistically significant ensemble of protein conformations starting from the available X-ray structure(s) is an important strategy for structure-based design. This approach has been tested on HIV-1 protease and has yielded promising results (Meagher and Carlson, 2004). A number of molecular dynamics (MD) simulation studies on the structural fluctuations of retroviral aspartic proteases have been published (Harte et al., 1990, 1992; Zhu et al., 2003; Levy and Caflisch, 2003; Levy et al., 2004; Perryman et al., 2004; Kovalskyy et al., 2004; Wittayanarakul et al., 2005; Meagher and Carlson, 2005), but the flexibility of free BACE has not yet been investigated by computational approaches.

In this study, twelve 300 K explicit-water MD simulations of BACE in the absence and presence of the inhibitor OM99-2 (total simulation time of $\sim$0.3 μs) were performed to investigate the plasticity of the binding site residues as well as the flap opening and the accompanying side chain reorientations. The simulations illustrate the dynamic properties of the binding site and provide structural insights into the role of individual active site residues and water molecules in catalysis. Moreover, the analysis of the trajectories suggests that the flap lacks a predominant conformation, an observation that has implications for inhibitor design.

Results and Discussion

Overview of the Simulations

To reduce statistical artifacts due to the choice of the starting conformation, several explicit solvent MD simulations were run by using the structure complexed with the peptidic inhibitor OM99-2 (Hong et al., 2000) and the two apo structures (Hong and Tang, 2004; Patel et al., 2004). Moreover, multiple trajectories with different initial atomic velocities were performed to improve conformational sampling (Caves et al., 1998). The names of the different runs are listed and explained in Table 1. Excluding the flexible insertion segments, the average C_α-rmsd from the corresponding X-ray structures ranges between 1.3 Å and 1.8 Å (Table 1) for the last 10 ns of the simulations, while the range for all C_α atoms is between 1.7 Å and 3.4 Å. The overall conformation (Figure 2A) and secondary structural elements are stable in all simulations.

Table 1. The Simulation Systems

Starting Structure	OM99-2 (1fkn)					APO1 (1sgz)	APO2 (1w50)
Inhibitor	Bound		Removed			absent	absent
Crystal waters	included	removed	removed	included	included	included	included
Sim. name[a]	om99-b	om99-b*	om99-u*	om99-u	om99-Cu	apo-u1	apo-u2
Sim. length[b] (ns)	33	22, 20	23, 20, 20	27, 27	31	32, 23	21
C_α-rmsd[c] (Å)	1.5	1.8, 1.5	1.7, 1.8, 1.8	1.8, 1.6	1.8	1.3, 1.3	1.7

Coordinates of inhibitor bound (1fkn [Hong et al., 2000]) and free (1sgz [Hong and Tang, 2004] and 1w50 [Patel et al., 2004]) structures were downloaded from the Protein Data Bank (Berman et al., 2000). OM99 and om99, as well as APO and apo, refer to the crystal structure and the name of the simulation, respectively.

[a] Individual trajectories differing only in the random assignment of the initial velocities are specified with A, B, or C in the text, e.g., om99-uA and om99-uB. Asp32 was protonated at the inner oxygen, except for om99-Cu, in which both Asp32 and Asp228 were deprotonated (Rajamani and Reynolds, 2004) (see text).

[b] Multiple trajectories are separated by commas.

[c] C_α-rmsd from the starting X-ray coordinates averaged over the last 10 ns of each simulation, excluding insertion segments. Multiple trajectories are separated by commas.

Motion in the Substrate Binding Site

On the basis of kinetic studies, multiple conformations of the active site region have been postulated for pepsin (Marcinkeviciene et al., 2002) and BACE (Toulokhonova et al., 2003). The heavy-atom rmsd of the 32 residues in the binding site is plotted in Figure 2B. While the heavy-atom rmsd does not exceed 1.6 Å in the bound simulation (black), its magnitude and fluctuation in the free simulations indicate major conformational changes, as previously observed in HIV-1 protease (Zoete et al., 2002). The rmsd of the heavy atoms of the binding site averaged over the last 10 ns is 2.4, 2.1, 2.2, 2.1, and 2.6 (±0.2) Å for om99-uA, om99-uB, apo-u1A, apo-u1B, and apo-u2, respectively, and these deviations are larger than the corresponding value of 1.5 ± 0.1 Å in om99-b. As an example, the flap opens significantly after about 6 ns in om99-uA, and even more than the aperture observed in the recent crystallographic structure of the native enzyme (Patel et al., 2004). Overall, the analysis of the trajectories suggests that the substrate binding site, particularly the tip of the flap, sampled large regions of conformational spaces in the free simulations, irrespective of the starting coordinates. On the other hand, the flap remained "closed" in the three bound simulations, and both the hydrogen bonding and van der Waals interactions between BACE and the OM99-2 inhibitor were maintained. In fact, the inhibitor, and in particular its P_4–P_2' segment, is tightly bound to the protein by up to 13 hydrogen bonds and more than 20 carbon-carbon contacts with a distance of less than 4 Å during the bound simulations (Figure 1B). Interestingly, the two C-terminal residues of the inhibitor show the largest fluctuations during the bound simulations, in agreement with their high average B factors (56.7 Å for P_3'-Glu and 71.9 Å for P_4'-Phe as compared to 27.4, 22.6, 21.5, 23.7, 24.7, and 29.7 Å for residues P_4–P_2', respectively [Hong et al., 2000]).

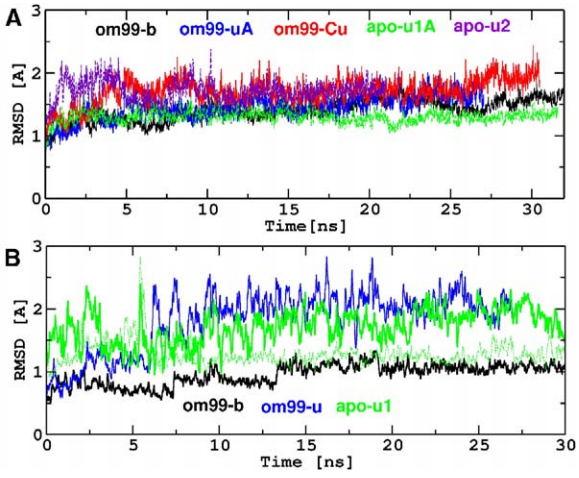

Figure 2. Structural Deviation in the MD Trajectories

(A) C_α-rmsd measured from the corresponding X-ray starting structure excluding insertion segments.

(B) Heavy-atom rmsd of the 32 binding site residues, i.e., those residues with at least one heavy atom within 5.0 Å of any heavy atom of the inhibitor OM99-2 in the 1fkn crystal structure (10–13, 30, 32, 34, 35, 69–73, 75, 108, 110, 118, 126, 128, 198, 223, 224, 226, 228, 230–233, 235, 307, 325, and 329). Dotted lines represent rmsd measured from the 1fkn crystal structure.

Motion in the Insertion Segments

Sub-ns motions were observed in the homodimeric aspartic protease of HIV-1 (Freedberg et al., 2002). Disordered regions were also observed in the X-ray structures of BACE (Patel et al., 2004). Despite the small deviations in the segments that are common to other aspartic proteases, almost all of the insertion segments (Figure 1A), particularly A (residues 158–167) and F (residues 311–318), experienced substantial displacement from their starting conformation. The observed flexibility is consistent with the X-ray data. In fact, segment A contains a short helix (residues 161–169) in the structures solved by Hong and colleagues (Hong et al., 2000, 2002; Hong and Tang, 2004; Turner et al., 2005), but it is not present in the liganded and unliganded structures reported by Patel et al. (Patel et al., 2004). In the simulations, besides the helix-to-loop interconversion, segment A as a whole underwent a large displacement away from the active site (e.g., up to 20 Å in om99-uB, Figure 3A). The displacement was concomitant to the loss of hydrogen bonds involving the carbonyl oxygen of Leu161 and the Gln163 side chain in segment A with side chains of Lys9 and Gln12 in the 10s loop. The con-

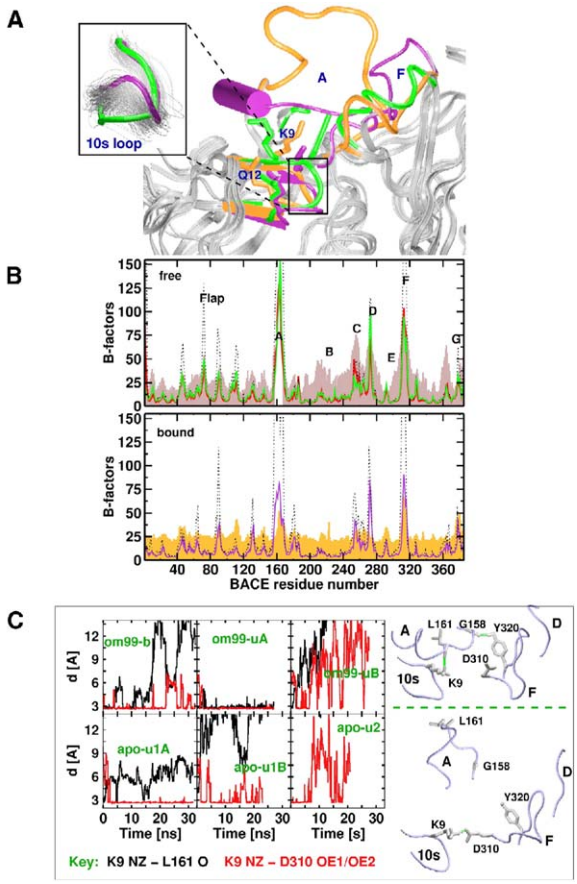

Figure 3. Backbone Flexibility

(A) Structure of OM99-2 (purple), APO2 (green), and a snapshot at 19 ns of simulation om99-uB (orange), showing the displacement of segment A, loop F, and the 10s loop (residues 9–14). Residues in the 10s loop involved in hydrogen bonding with residues in segment A are in sticks. Part of the protein is shown in gray ribbons. Segments A and F were excluded from the C_α superposition. Inset, snapshots (gray lines) of the 10s loop at 100 ps resolution. The view in the inset is slightly rotated with respect to the orientation in (A).

(B) Temperature factors of C_α atoms in Å^2 computed from the root mean square fluctuations (rmsf) as $B = 8\pi^2/3\ rmsf^2$ and averaged (excluding the first 10 ns) over intervals of 1 ns (solid lines) and 10 ns (dotted lines). In the upper panel, the combined averages from the inhibitor-free simulations containing the crystal waters (om99-u in red, and apo-u1 plus apo-u2 in green) are compared with the experimental B factors in the free BACE X-ray structure of APO2 (Patel et al., 2004) (brown). Note that segment A is disordered and therefore not observed in the APO2 X-ray structure. The flap (residues 67–77) and all insertion segments are labeled. In the lower panel, B factors from the inhibitor bound simulation (om99-b in violet) are compared with the B factors reported in the OM99-2 X-ray structure (Hong et al., 2000) (orange).

(C) Time evolution of some of the hydrogen bonds of Lys9. Lines in some of the plots are out of range and not visible. The snapshots on the right show the pattern of hydrogen bonds at 0.1 ns (top) and 17.5 ns (bottom) of simulation om99-uB.

formational change of the 10s loop is not as large, lying between the OM99-2 and APO2 X-ray structures (Figure 3A, inset). Loop F is also spatially close to the 10s loop and is disordered in all of the X-ray structures (Hong et al., 2000, 2002; Hong and Tang, 2004; Turner et al., 2005; Patel et al., 2004), as is the case in the simulations (Figure 3A). The mobility of the insertion segments A and F could have functional significance, as their outward movement opens the S_3 subpocket. The crystallographic B factors and the corresponding values derived from the root mean square fluctuations (rmsf) averaged over intervals of 1 ns (excluding the first 10 ns) are compared in Figure 3B. The solvent-exposed insertion segments A, D (residues 270–273), and F in the C-terminal lobe (residues 151–385) of the enzyme are very flexible. Their mobility is in accord with the distribution of temperature factors in the apo structure (Patel et al., 2004). At a longer time interval of 10 ns (dotted lines), the motion of the flap, segment A, loop F, and residues 87–92 increased significantly. It is important to note that the MD simulation results show that the higher flexibility of the C-terminal lobe is intrinsic to the BACE structure and is not due to fewer crystal contacts with symmetry-related molecules as suggested previously (Patel et al., 2004).

The fluctuations observed in the simulations of uncomplexed BACE started from the inhibitor bound or the apo X-ray structures are very similar (Figure 3B, green and red in the upper panel). Furthermore, simulations with and without ligand also exhibit similar flexibilities, the only major difference being the lack of fluctuations in the flap (residues 67–77) during the bound simulations. The motion of the flap in the free enzyme is due to the loss of interactions with both the inhibitor and other parts of the protein (e.g., Tyr71-Trp76 hydrogen bond, see below). As pointed out earlier, the loss of hydrogen bonds of segment A with the 10s loop in the active site pocket is related to the outward motion of segment A (Figure 3A), which affects the nearby loops F and D. The backbone carbonyl of Leu161 in segment A competes with Asp310 near the N terminus of loop F for a hydrogen bond with the side chain of Lys9 in the 10s loop (Figure 3C). Indeed, in the simulations, the Lys9-Asp310 side chain hydrogen bond is more stable than the Lys9-Leu161 hydrogen bond, in agreement with the APO2 X-ray structure in which A was entirely missing and the 10s loop was displaced by 4.5 Å with respect to OM99-2. Only in om99-uA is the hydrogen bond between the carbonyl of Leu161 and the Lys9 side chain stable (Figure 3C); here, segment A also retains the conformation of the starting structure. Furthermore, the backbone carbonyl of Gly158 (segment A) is close to the phenolic OH of Tyr320 (near the C terminus of segment F) in the APO1 and OM99-2 X-ray structures, but not in the simulations and APO2 (Figure 3C, right). Despite the uncertainties that can arise from experimental conditions such as crystal packing and disorder contributions, the very good overall agreement between crystallographic and calculated B factors indicates that the relative flexibility of the different parts of the protein is correctly captured in the simulations.

Intralobe Concerted Motion

To investigate concerted motion in BACE, the crosscorrelation coefficient between the displacement of each pair of residues was calculated following a previous

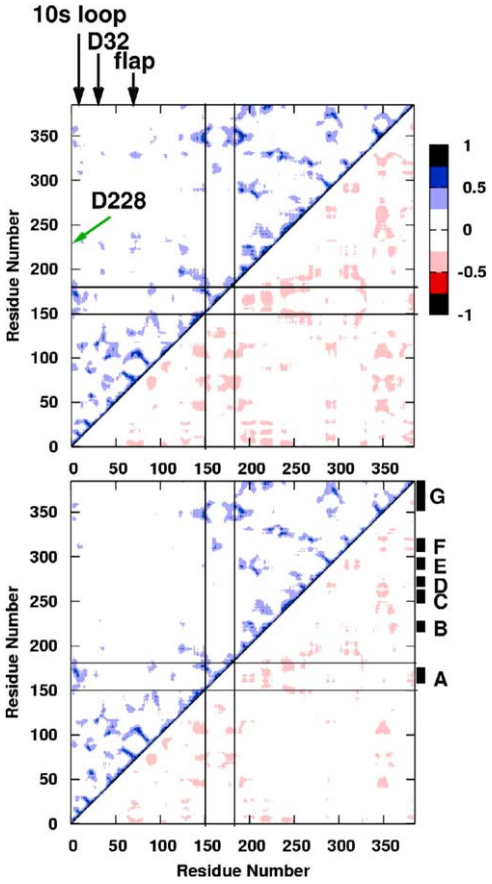

Figure 4. Correlated Motion in BACE

The crosscorrelation coefficient C_{ij} between the displacement of C_α atoms i and j is calculated as $C_{ij} = \langle \Delta\vec{r}_i \Delta\vec{r}_j \rangle / (\langle \Delta r_i^2 \rangle \langle \Delta r_j^2 \rangle)^{1/2}$ where $\Delta\vec{r}_i$ is the displacement from the average position of C_α atom i, and $\langle\,\rangle$ represents an average over a simulation segment (Harte et al., 1990). Data were obtained by averaging the C_{ij} over 170 segments of 0.1 ns each. The last 17 ns of the trajectories om99-b (top) and om99-uA (bottom) were used for this plot, and very similar patterns are observed for other trajectories (see text). In each plot, the upper and lower triangles show correlated and anticorrelated displacement, respectively. The black solid lines emphasize the interfacial region.

analysis of HIV-1 protease dynamics (Harte et al., 1992; Zoete et al., 2002). Backbone motion is correlated within each lobe of BACE (Figure 4). Moreover, part of the interfacial region, i.e., residues 151–180, moves in concert with the rest of the protein, which is essential to preserve integrity of the active site. On the other hand, the insertion segments do not show a positively correlated motion with the rest of the structure. The inhibitor bound and free simulations display a similar pattern of concerted motion, except for the higher correlation in the former, which can be explained by the increased rigidity of the enzyme due to the presence of a tightly bound peptide in the binding site between the two lobes. In other words, the inhibitor acts as an interlobe "communicator," which is not possible for the water molecules occupying the binding site in the free enzyme. In fact, the segments with higher correlation in the bound with respect to the free simulations are the catalytic dyad, 10s loop, and the flap (Figure 4). As previously found for HIV-1 protease (Harte et al., 1992), correlated motion is higher at longer timescales, but the pattern is essentially identical (not shown). The present analysis, and in particular the intralobe concerted motion, is consistent with a comparative study of the X-ray structures of native endothiapepsin and 15 endothiapepsin-inhibitor complexes, which suggested that there are few interactions between the two parts of this enzyme and, therefore, they can undergo displacement "as separate rigid bodies" (Šali et al., 1992). On the other hand, it is difficult to directly compare with the correlated motion in HIV-1 protease because of the short simulation lengths used for previous analyses (Harte et al., 1992; Zoete et al., 2002).

Flap Opening in the Free Simulations

In the inhibitor bound conformation, the active site cleft of eukaryotic aspartic proteases is covered by a long β hairpin, and the phenolic OH of the flap residue Tyr71 is involved in a hydrogen bond with the side chain NH of Trp76 (Tyr75 and Trp39, respectively, in pepsin numbering). The flap-open conformation is characterized by a displacement of the flap away from the catalytic aspartates and the absence of the Tyr71-Trp76 hydrogen bond (Patel et al., 2004). The flap-open conformation has been observed in penicillopepsin (3app), the monoclinic crystal form of saccharopepsin (1fmx), and BACE (1sgz and 1w50). Moreover, extensive experimental and computational studies on HIV-1 protease have shown that both open- and closed-flap conformations are accessible to the retroviral enzyme (Harte et al., 1990, 1992; Collins et al., 1995; Ishima et al., 1999; Freedberg et al., 2002; Katoh et al., 2003; Levy and Caflisch, 2003; Levy et al., 2004; Clemente et al., 2004; Perryman et al., 2004).

While in the simulations with the peptidic inhibitor (om99-b and om99-b*) the Tyr71-Trp76 side chain hydrogen bond was stable, and the flap remained tightly closed with a minor motion at the tip (Figure 3B), a wide range of flap positions were observed in the simulations without the inhibitor. Structural clustering (see Experimental Procedures) based on the C_α atoms of the residues near the flap tip (69–75) was used to quantify the most populated conformations. Clustering of the combined snapshots (excluding the first 10 ns) from the two trajectories of om99-u yielded two major clusters, each populated at ~48%, representing the flap-open (blue) and flap-closed (orange) configurations (Figure 5, top left). The same procedure applied to the three trajectories started from the apo structures produced a cluster with 84% population of closed-like conformations (Figure 5, top right, blue) and a minor cluster (~10%) containing the open-flap conformations (orange). Thus, both the open- and closed-flap conformations of BACE are accessible within a 10 ns timescale. The simulation results suggest that the potential energy surface of free BACE is characterized by many local minima with small energetic differences, some of which are sampled by molecular dynamics at 300 K.

Although the presence or loss of the Tyr71-Trp76 hydrogen bond is observed in both the open- and closed-flap conformations (Figure 5), the open-flap conforma-

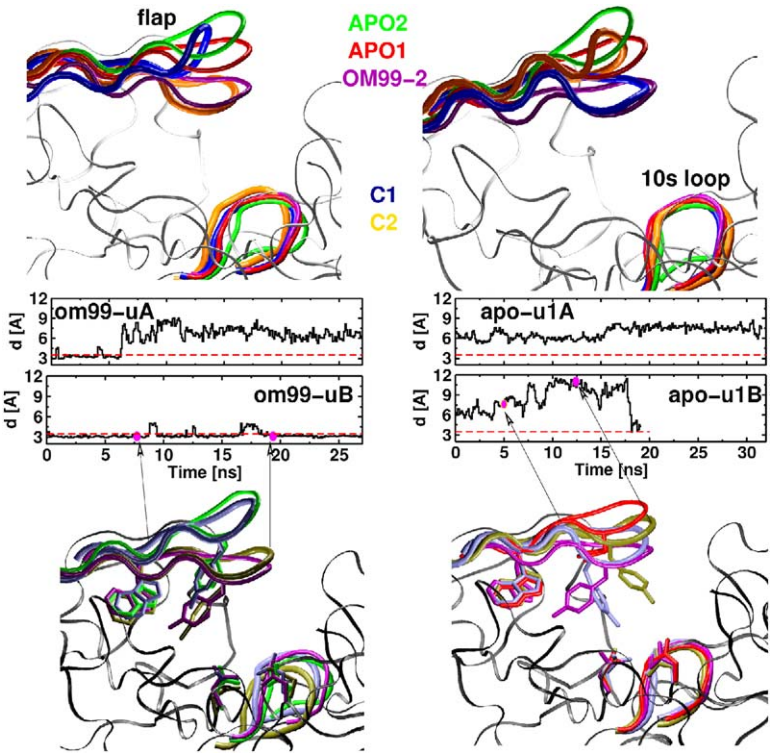

Figure 5. Representative Conformations of the Flap and the 10s Loop

(Top) Center of the two most populated clusters C1 (blue) and C2 (orange). Snapshots collected at 10 ps intervals along simulations om99-u (left) or apo-u1 and apo-u2 (right) were combined (excluding the first 10 ns) and clustered based on C_α-rmsd of the flap residues and a cutoff of 1.0 Å. All C_α atoms, except for the flexible flap and segments A, D. and F, were used in the structural fitting prior to clustering. Superposition of the displayed cluster centers and snapshots onto the X-ray structures OM99-2 (magenta), APO1 (red), and APO2 (green) was based on C_α atoms, excluding residues 155–170, which are not present in APO2. The time evolution of the distance *d* between the hydroxyl oxygen of Tyr71 and the indole nitrogen of Trp76 is plotted for four of the trajectories used in the clustering (see Figure 7 for apo-u2, which is not shown here). The red dashed-line at 3.5 Å represents a hydrogen bond cutoff. (Bottom) The snapshots selected from the inhibitor-free simulations show that the Tyr71-Trp76 side chain hydrogen bond can be present (left) or absent (right) in the open-flap conformation. In the latter case, the Tyr71 side chain can assume multiple orientations.

tion has a longer life time (within the simulation timescales of 20–30 ns) when the Tyr71-Trp76 hydrogen bond is irreversibly broken (om99-uA). The open-flap conformation is not significantly populated when the hydrogen bond is formed (om99-uB). Furthermore, during the displacement of the flap from the open- to the closed-form observed in simulation apo-u2, the Tyr71-Trp76 hydrogen bond formed at 14 ns. Therefore, the open-flap conformation with the Tyr71-Trp76 hydrogen bond as well as the closed-flap conformation without the hydrogen bond appear to be transient. Ligand design based on representative structures with open flap without the Tyr71-Trp76 hydrogen bond may lead to novel BACE inhibitors. A precedent exists in the binding of a 3,4-disubstituted piperidine to renin, where loss of the flap hydrogen bond and side chain displacements were observed by X-ray crystallography (Oefner et al., 1999).

The curling of the flap tip (Figure 5) correlates with changes in the angle between the C_α atoms of the flap tip residues Tyr71, Thr72, and Gln73 (not shown), as was previously observed in HIV-1 protease (Perryman et al., 2004). The separation between the bottleneck residues Thr72 at one side and Arg235, Ser328, and Thr329 at the other side of the active site cleft was previously used as a criterion for flap opening (Hong and Tang, 2004). Here, three variables are defined for a detailed description of the motion and orientation of the flap (Figure 6A): Z monitors the distance of the flap tip from the catalytic aspartic acid residues, X measures the gap between the flap tip and the loop facing it from the C-lobe, and Y measures the distance between the side chains of the bottleneck residues. The variable Y, though similar to X, considers side chain orientations and provides the narrowest point of flap opening (e.g., 3.5 Å and 4 Å in the X-ray structure OM99-2 and during the om99-b simulation, respectively [Table 2]). It is clear from the scatter plots in Figure 6 that there is a substantial difference in flap motion (and opening) between the inhibitor bound (Figure 6B) and free simulations (Figures 6C and 6D). Each of the free trajectories sampled both the open and closed conformations irrespective of the starting structure or the active site protonation. However, details of the flap motion varied, consistent with the different levels of opening observed in the X-ray structures APO1 and APO2. Relative to the starting coordinate, the flap in both om99-u simulations moved higher up (larger Z) and farther away from the loop opposite it (larger X). Also, the juxtaposed bottleneck residues moved farther apart (larger Y). In apo-u1, the scatter plots (Figure 6D) are inverse-bell shaped, indicating that no further closure of the bottleneck beyond the closure observed in OM99-2 is possible, yet the flap tip can move toward the S_1 pocket (lower Z). Such displacement of the flap tip is most pronounced in the simulations with both of the catalytic aspartates charged (om99-Cu) and in the runs without the crystal waters (om99-u*). The latter observation might be related to the lack of a water molecule in the position of the conserved W2 (see below) at the beginning of the om99-u* runs. The same observation provides evidence that it is more appropriate to keep the water molecules of the crystal structure in MD simulations because equilibration of water molecules into binding site pockets is not complete within a 20 ns timescale.

The extent of flap opening differs not only between

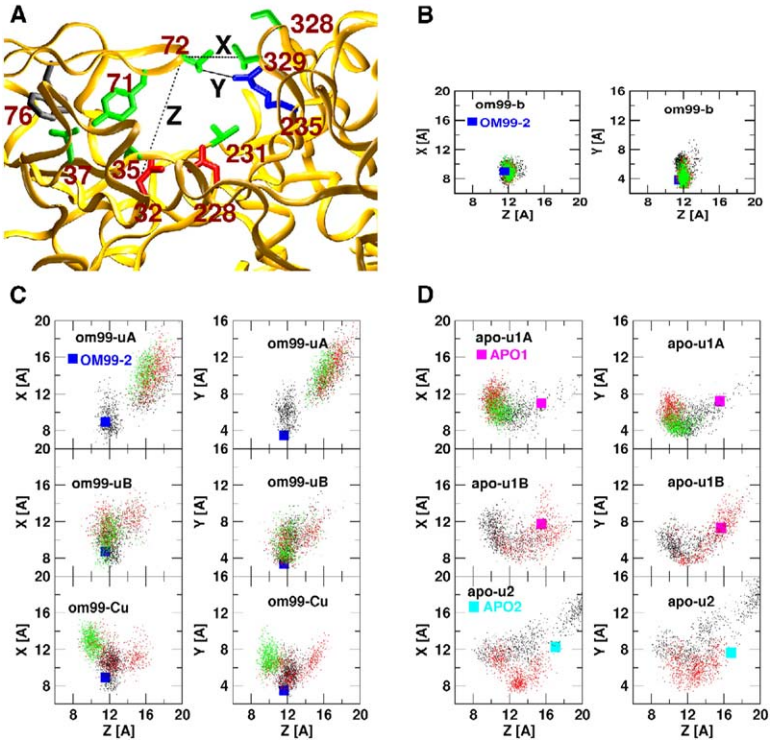

Figure 6. Structure of the Active Site of BACE

(A) Residues important for function and flap opening are represented by a stick model, labeled by the sequence number, and colored in red (acidic), blue (basic), green (polar), and gray (Trp76). The following (minimum) distances are emphasized by dotted lines: Z, between the Cα of the flap tip residue Thr72 and the Cβ of one of the catalytic aspartates; X, between the C_α atoms of Thr72 at one side and Thr329 on the other side of the active site cleft; and Y, between the Thr72 and Arg235 side chains. Thr72 and Arg235 were selected for Y because their separation monitors the narrowest point of flap opening, and both side chains interact with inhibitors.

(B–D) Scatter plots of X and Y versus Z. The black, red, and green dots indicate simulation segments 0–10 ns, 10–20 ns, and 20–30 ns, respectively.

two simulations with different starting structures (e.g., between om99-u and apo-u1), but also between two simulations started from the same structure (e.g., between om99-uA and om99-uB or between apo-u1A and apo-u1B). Note that the latter pairs differ only in the assignment of random values for the initial velocities and that multiple trajectories were performed to improve sampling (Caves et al., 1998). The combined averages of the data from the same set of simulations resulted in values similar to those measured on the X-ray structures. The values of the variables X, Y, and Z over the last 10 ns of the two om99-u simulations are in excellent agreement with the crystallographic apo structures (Table 2). For apo-u1 and apo-u2, the average values of X, Y, and Z are between those of the apo and inhibitor bound X-ray structures. Moreover, the histograms of Z and Y in Figure 7A show that the peaks are sharp and narrow in the bound simulations (dashed lines), but are wide and shallow in the free simulations.

Hong and Tang reported that an opening of the bottleneck by 6.5 Å is sufficient for the active site entrance of the 8 residue peptidic inhibitor OM00-3 (Hong and Tang, 2004). The simulations show that in solution there is a wide range of flap positions in free BACE that allows active site entrance of small-to-large substrates. The availability of several alternative configurations of the binding site could also allow for different substrates to bind, providing a possible explanation for the broad specificity of BACE (Grüninger-Leitch et al., 2002). Whether the motion of the flap tip into the active site (as measured by Z in om99-Cu and om99-u*) has a functional role is yet to be determined.

Self-Inhibition and Orientation of the Flap Tyrosine

The orientation of the Tyr71 side chain was monitored along the simulations by using the angle θ between the vectors Tyr71 C_β → Tyr71 OH and Tyr71 OH → Gly34 O (Figure 8A). Thus, θ is large (small) for Tyr71 orientations pointing toward (away from) the S_1 pocket. In the bound

Table 2. Flap Displacement

	Simulation							X-Ray Structure		
	om99-b	om99-b*	om99-u*	om99-u	om99-Cu	apo-u1	apo-u2	OM99-2	APO1	APO2
<Z>	12.0 ± 0.3	12.7 ± 0.8	10.6 ± 1.1	14.1 ± 2.3	10.1 ± 0.4	12.6 ± 2.6	12.7 ± 2.7	11.6	15.5	16.7
<X>	9.0 ± 0.7	9.4 ± 1.5	9.1 ± 1.0	12.5 ± 1.7	12.8 ± 0.9	11.1 ± 1.3	9.6 ± 1.9	8.8	11.0	12.2
<Y>	4.3 ± 0.9	4.0 ± 0.6	4.8 ± 1.0	8.0 ± 3.0	7.0 ± 1.2	6.6 ± 1.6	6.0 ± 1.7	3.5	7.1	7.7
<D>	9.9 ± 2.2	10.5 ± 1.6	11.1 ± 1.1	11.2 ± 1.2	9.3 ± 0.8	11.2 ± 2.2	9.1 ± 1.5	9.6	2.9	7.4

Time-averaged distances and standard deviations over the last 10 ns. All values are in Angstroms. In the case of multiple trajectories, the last 10 ns of each was used to obtain a combined average. See the legend of Figure 6 for the definition of Z, X and Y. *D* is the distance between Tyr171(OH) and Lys107(O). ⟨⟩ represents the time average. The last three columns contain values of Z, X, Y and *D* measured on crystal structures.

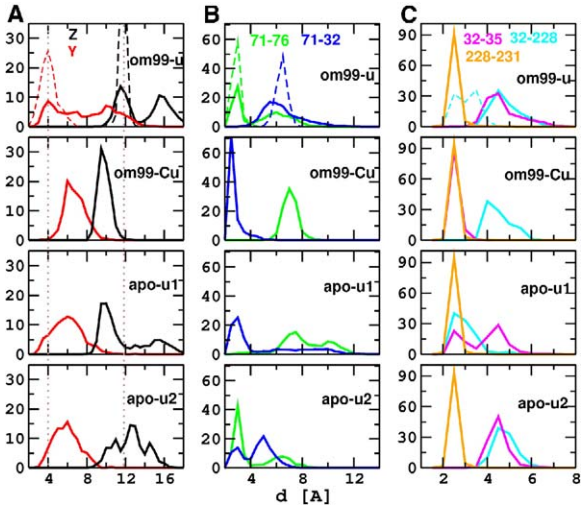

Figure 7. Histograms of Distances between Selected Residues around the Active Site

(A–C) The y axis represents the percentage of snapshots saved during the last 10 ns of individual simulations. Data for the free and om99-b inhibitor bound simulations are plotted with solid and dashed (only top) lines, respectively. (A) The distance between Cα of Thr72 and Cβ of Asp32 and the minimum distance between the side chain heavy atoms of Thr72 and Arg235 are shown in black and red (same as Z and Y in Figure 6A), respectively. The dotted vertical lines are for guiding the eye to the peak of Z and Y in om99-b. (B) The distance between the hydroxyl oxygen of Tyr71 and the indole nitrogen of Trp76 in green (*d* in Figure 5), and the carboxyl oxygen of Asp32 in blue. (C) Minimum distance between the functional groups of Asp32 and Ser35 in magenta, between Asp32 and Asp228 in cyan, and between Asp228 and Thr231 in orange.

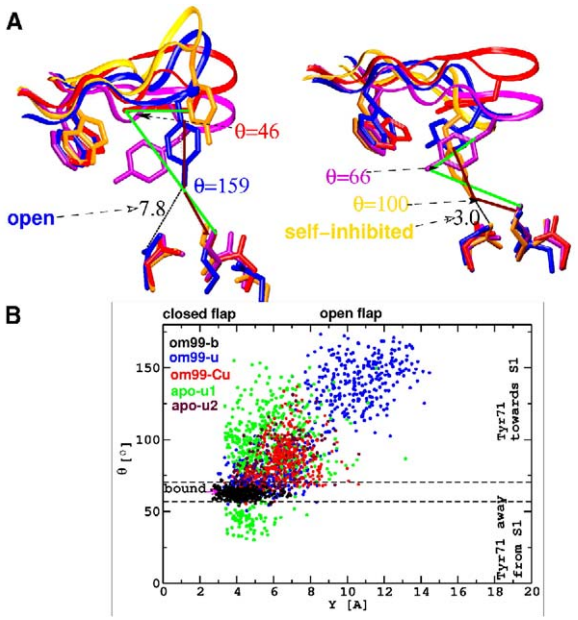

Figure 8. Orientation of Tyr71 and Self-Inhibition

(A) Tyr71, Trp76, Gly34, Asp32, and Asp228 (sticks) and the flap (tubes) in the OM99-2 and APO1 X-ray structures (color codes are as in Figure 5). Blue and orange represent the center of the two most populated clusters in om99-u (left) and apo-u1 (right). Here, conformations were clustered by using the backbone rmsd of residues 20 Å around Asp32 Oδ1 and a cutoff of 1.2 Å. The angle θ (see text) is emphasized with green and brown solid lines and is labeled for some of the conformations. The minimum distance between the hydroxyl oxygen of Tyr71 and either carboxyl oxygen of Asp32 is also shown for one of the two most populated clusters (black dotted lines).

(B) A scatter plot of θ against the variable Y (see text).

simulations, θ remained around 60°, while it significantly increased in the unbound simulations upon rupture of the Tyr71-Trp76 hydrogen bond (om99-u) or the hydrogen bond between Tyr71 OH and the CO of Lys107 (apo-u1, Figure 8B). Thus, the side chain of Tyr71 in the free simulations generally points toward the S_1 substrate binding pocket. Furthermore, in the conformations in which the flap tip is also oriented toward the S_1 pocket (i.e., those with smaller values of variable Z, such as in apo-u1, in om99-Cu, and, to some extent, in apo-u2), the Tyr71 side chain is involved in a direct hydrogen bond with the side chain carboxyls of Asp32 (Figures 7B and 8) or with the backbone carbonyl of Gly34 in a self-inhibitory mode. Note, however, that the Tyr71-Asp32 hydrogen bond was reversible and weak in simulations apo-u2 and apo-u1B. Hence, the self-inhibited form is not the dominant conformation when the catalytic dyad is monoprotonated. Moreover, apo-u2 evolved to the closed-flap conformation with eventual formation of the Tyr71-Trp76 hydrogen bond. The Tyr71-Asp32 interaction is strongest in om99-Cu, since the hydroxyl of Tyr71 was further stabilized by the stronger negative potential in the active site. This result supports the monoprotonation of the active aspartates and is consistent with the reduced activity of BACE around neutral pH (Vassar et al., 1999; Grüninger-Leitch et al., 2002).

The self-inhibited conformation observed in the simulations is similar to the X-ray structures of the wild-type (Gilliland et al., 1990; Newman et al., 1991) and the Val111Phe variant (Strop et al., 1990) of free chymosin, as well as the trigonal crystal form of free saccharopepsin (Gustchina et al., 2002). In these structures, Tyr75 (pepsin numbering) is in either a direct or a water-mediated hydrogen bonding arrangement with the carbonyl oxygen of Gly217 (corresponding to Gly34 in BACE). Despite suggestions of some functional role, such as having a negative impact on activity (Gustchina et al., 2002), the importance of self-inhibition in catalysis is not known. Based on the calculated pK_as (see Experimental Procedures), both Asp32 and Asp228 are likely to be charged at neutral pH. Thus, the deprotonation of the aspartates in simulation om99-Cu roughly represents the active site charge distribution around neutral pH. Therefore, although insufficient statistics precludes a definitive claim, the om99-Cu simulation results indicate that self-inhibition by the displacement of the Tyr71 side chain into the S_1 pocket impairs the enzymatic activity at neutral pH. This is consistent with the fact that aspartic proteases often employ conformational changes to modulate their intrinsic activity. In Cathepsin D, a 10 residue N-terminal segment relocates into the active site so that an interaction of a lysine

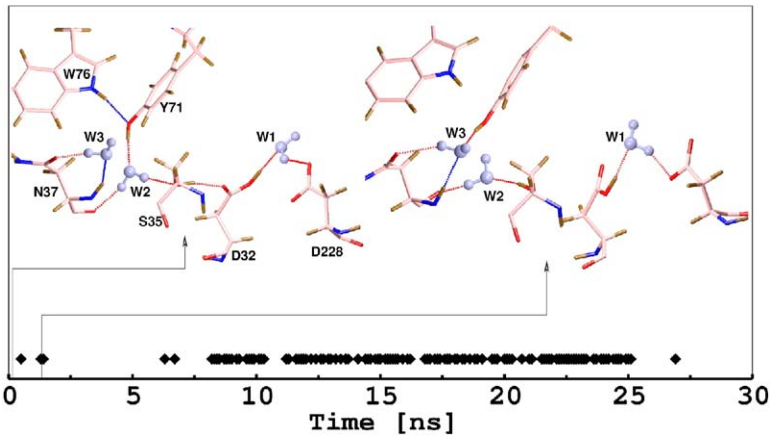

Figure 9. Hydrogen Bond Donor and Acceptor Role Swapping between W2 and Ser35 during the Free Simulations

Diamonds represent snapshots from om99-uA (in 100 ps resolution) in which the Ser35 hydroxyl acts as a donor to W2. Snapshots before (left) and after (right) the switch in the donor/acceptor roles of W2 are shown. A third water molecule (W3) near W2 stabilizes Asn37. Hydrogen bonds are shown by dotted lines, amino acids are shown by sticks, and water molecules are shown by ball-and-sticks.

residue at position 7 with the catalytic aspartates blocks proteolytic activity at neutral pH (Lee et al., 1998). A very recent crystallographic study on allergen Bla g 2, a Zn binding aspartic protease that lacks substantial proteolytic activity, revealed that the enzyme is self-inhibited by direct contacts between a phenylalanine side chain in the flap (corresponding to Tyr71 in BACE) and the catalytic residues (Gustchina et al., 2005).

As mentioned above, the side chain of Tyr71 is involved in an unusual hydrogen bond with the carbonyl oxygen of Lys107 in the APO1 structure (Hong and Tang, 2004). This hydrogen bond was not observed in simulations from OM99-2 or APO2, and it broke early (5 and 10 ns) in the two simulations started from APO1 itself (Table 2). Thus, the conformation of the Tyr71 side chain in APO1 is not consistent with other structural data (Patel et al., 2004) and the present simulation results. One possible explanation may be that the catalytic pocket of APO1 was occupied by impurities that probably forced the side chain of Tyr71 to point outside of the substrate binding site. In fact, upon superposition of the electron density maps onto the APO1 atomic coordinates (pdb code 1sgz, structure factors kindly provided by Dr. L. Hong), a weak electron density is visible in the active site. Hence, it is likely that the hydrogen bond between Tyr71 and the CO of Lys107 is present only sporadically in the free enzyme.

Interactions in the Active Site

Two conserved water molecules in the active site of aspartic proteases play a crucial role in function and stability (Andreeva and Rumsh, 2001; Prasad and Suguna, 2002). The catalytic water (W1) bridges the two catalytic aspartates and is involved in the nucleophilic attack. The minimum distance between the carboxyl oxygens of the catalytic Asp dyad averaged over the last 10 ns is ~2.5–3.5 Å and ~4.5 Å in the bound and unbound simulations, respectively (Figure 7C). These distances indicate that hydrogen bonding between Asp32 and Asp228 is possible in the presence of a substrate (i.e., in a flap-closed conformation), but that it is mediated by W1 after flap opening.

Another water molecule (W2) stabilizes the flap-closed conformation by participating in a network of hydrogen-bonded residues Trp76-Tyr71-W2-Ser35-Asp32 (Figure 9, left). In the bound simulations, the Tyr71 hydroxyl acts as an acceptor for the NH of Trp76 and donates to W2. As a consequence, W2 is oriented such that it acts as a donor to the Asn37 backbone carbonyl and the Ser35 side chain hydroxyl. Thus, the hydroxyl of Ser35 is polarized to act as a donor to the anti-lone pair of the outer oxygen atom of Asp32. Moreover, the Asn37 NH and the side chain CO are involved in hydrogen bonds with another water molecule (W3). Interestingly, the Asp32-Ser35 hydrogen bond was not stable in the free simulations (Figures 7C and 9), consistent with the observation that in all of the X-ray structures lacking the Tyr71-Trp76 hydrogen bond, the distance between the carboxyl group of Asp32 and the hydroxyl functionality of Ser35 is larger than in the presence of the Tyr71-Trp76 hydrogen bond (Andreeva and Rumsh, 2001). It is important to note that the rupture of the hydrogen bond between Ser35 and Asp32 takes place concomitantly with the W2 reorientation so that W2 can act as an acceptor for the Ser35 hydroxyl while still donating to the backbone carbonyl of Asn37 (Figure 9). Such a spontaneous reorientation is also in accord with the thorough structural analysis of Andreeva and Rumsh who postulated that W2 and Ser35, which are conserved in all pepsin-like enzymes, swap their donor and acceptor roles during the catalytic cycle (Andreeva and Rumsh, 2001). Most importantly, the Asp32-Ser35 interaction was intact in the simulation where both the active aspartates were charged (om99-Cu), indicating that the hydrogen bond switch described above is designed for function at low pH, as proposed (Andreeva and Rumsh, 2001).

In contrast to the Asp32-Ser35 interaction, the hydrogen bond between the Asp228 carboxyl and the Thr231 hydroxyl is very stable in all simulations (Figure 7C). Hence, the simulation results support the reaction mechanism proposed by Andreeva and Rumsh and in particular the role of residues around the active site, i.e., Thr231 protects the Asp228 carboxyl from protonation at acidic pH and Ser35 assists in proton acceptance and release by Asp32 during the catalytic cycle (see Figure 6 of Andreeva and Rumsh, 2001).

Conclusions

Multiple explicit-solvent MD simulations of free and inhibitor bound BACE were performed, with particular emphasis on the substrate binding site, to investigate its flexibility. The MD trajectories were analyzed and compared with most of the available crystallographic data on BACE, and a good agreement was found for both overall stability and thermal fluctuations. Three main results emerge from the simulations and complement the static picture derived from the experimental data. First, in the absence of inhibitor, the flap (residues 67–77) covering part of the substrate binding site is very flexible and can switch from the closed- to the open-conformation or vice versa on a 10 ns timescale at room temperature. The potential energy surface of BACE consists of multiple local minima in the neighborhood of the native structure that differ little in energy and are separated by low-energy barriers (Elber and Karplus, 1990). The intraflap Tyr71-Trp76 side chain hydrogen bond is observed in both the open- and closed-flap conformations, but it is more stable in the latter. Furthermore, the unusual hydrogen bond observed in one X-ray structure of free BACE (Hong and Tang, 2004) between the Tyr71 hydroxyl group and the backbone carbonyl of Lys107 is not stable. These simulation results suggest that BACE inhibitor design should make use of both the closed-flap conformation in the presence of the Tyr71-Trp76 side chain hydrogen bond and the open-flap conformation with multiple orientations of the Tyr71 side chain. This detailed information is useful for structure-based, computer-aided design, which is likely to play an important role in the discovery of BACE inhibitors (Huang et al., 2005). In fact, not a single BACE inhibitor was found in a library containing more than 1,800 renin inhibitors (Grüninger-Leitch et al., 2002), despite the fact that both BACE and renin are pepsin-like enzymes. Moreover, only a single molecule (1,3,5-trisubstituted benzene) emerged as a BACE inhibitor from a multimillion compound library submitted to a high-throughput in vitro screening campaign (Coburn et al., 2004). On the other hand, using high-throughput docking of a composite library of about half a milion compounds and continuum electrostatic calculations (Huang and Caflisch, 2004), we have recently identified 12 phenylurea derivatives (out of 72 compounds tested experimentally) that inhibit BACE in at least 1 of 2 different mammalian cell-based assays at concentrations lower than 10 μM (Huang et al., 2005). We plan to continue our in silico screening based on docking by using the present trajectories in a pharmacophore-type approach based on multiple BACE conformations. The utility of such an approach, and in particular the improved performance upon incorporation of protein flexibility, has been shown for HIV-1 protease by others (Meagher and Carlson, 2004).

Second, the Tyr71 side chain can be involved in a hydrogen bond with the catalytic Asp32 or the carbonyl oxygen of Gly34, which results in self-inhibition, especially at neutral pH, at which both catalytic aspartates are likely to be charged. This observation is consistent with a pH optimum of about 4 for BACE activity and poor activity at pH values above 6 (Grüninger-Leitch et al., 2002).

Third, the simulation results provide further evidence for the role, proposed previously by others (Andreeva and Rumsh, 2001), of the conserved water molecules and residues involved in hydrogen bonds with the aspartates of the catalytic dyad. In particular, the fast (i.e., sub-ns) reorientation of the Ser35 hydroxyl group and the rigidity of the Thr231 side chain indicate that the former assists Asp32 in proton acceptance and release during catalysis, while the latter protects the Asp228 carboxyl from protonation at acidic pH.

Experimental Procedures

Preparation of BACE

Coordinates of BACE in complex with the inhibitor OM99-2 (Glu-Val-Asn-Leu-ϕ[CHOH-CH2]-Ala-Ala-Glu-Phe, where ϕ[CHOH-CH2] is a hydroxyethylene isostere of the peptide bond) were downloaded from the pdb database (Berman et al., 2000) (PDB entry 1fkn [Hong et al., 2000]). Simulations were performed by using the A chain with and without the crystal waters and in the presence and absence of the inhibitor (Table 1). While this work was in progress, an X-ray structure of BACE without bound inhibitor (APO1) was published (PDB entry 1sgz [Hong and Tang, 2004]). The unique orientation of the Tyr71 side chain (see Introduction) prompted us to perform two simulations with APO1 as a starting structure (Table 1). Furthermore, yet another structure of free BACE was published recently (APO2, pdb code 1w50) (Patel et al., 2004). A simulation from APO2 was performed to improve statistics (Table 1).

Particular attention was given to the ionization state of the cleavage site, which contains the aspartyl dyad (Asp32/Asp228). At optimal pH for enzymatic activity (~3.5–4.5), the aspartyl dyad is most probably monoprotonated in the uncomplexed enzyme as well as in the complex with the peptidomimetic inhibitors with a hydroxyethylene isostere of the peptide bond. In this study, the pK_a values for the charged groups were calculated by using the finite-difference Poisson-Boltzmann method as in a previous work (Gorfe et al., 2002). Asp32 was protonated based on the computed pK_a on the OM99-2 X-ray structure (the estimated pK_as were 4.6 and 0.2 for Asp32 and Asp228, respectively). The protonation of Asp32 was also suggested by a previous MD and docking study (Park and Lee, 2003). A recent quantum mechanical study suggested dideprotonated and monoprotonated states for the free and complexed forms of BACE, respectively (Rajamani and Reynolds, 2004). However, dideprotonation is in contradiction with the accepted reaction mechanism of pepsin-like enzymes (Suguna et al., 1987; Davies, 1990), which requires that one of the aspartic residues be protonated. To check the behavior of the simulations in the dideprotonated state of the unligated enzyme, a simulation was run in which both Asp32 and Asp228 were charged (Table 1).

Molecular Dynamics Simulations

The protein was solvated in a water box of appropriate dimensions so that the minimum distance between any protein atom and the side of the box is 13 Å, resulting in ~15,535 water molecules and a total number of atoms of ~52,000. The water molecules were equilibrated around the rigid protein for 0.2 ns. The isothermal isobaric ensemble with Berendsen temperature control (a coupling constant of 0.4 ps) and Nose-Hoover pressure control (Hoover, 1985), full particle-mesh Ewald electrostatic (Essmann et al., 1995), a 12 Å cutoff for vdW interactions, and a time step of 2 fs were used in all simulations. The simulation systems contained 11 (or 12 in om99-Cu) Na ions to compensate for the net negative charge of BACE. The simulations were performed by the program NAMD2 (Kalé et al., 1999) with the CHARMM22 (MacKerell et al., 1998) force field and TIP3 water parameters, and the trajectories were analyzed by the programs CHARMM (Brooks et al., 1983), VMD (Humphrey et al., 1996), and an in-house trajectory analysis tool (WORDOM, M. Seeber et al., personal communication). The leader algorithm (Hartigan, 1975; Settanni et al., 2005) was used for structural clustering based on the rmsd of selected atoms.

Names of the simulations are listed in Table 1. Individual trajecto-

ries are suffixed with A, B, or C (e.g., om99-uA, om99-uB, apo-u1A, apo-u1B, etc.).

Acknowledgments

We are grateful to D. Huang, M. Cecchini, R. Pellarin, and Dr. R. Böckmann for useful discussions, Drs. L. Hong and J. Tang for providing the structure factors for one of the X-ray coordinates, and Dr. S. Jelakovic for the analysis of electron density maps. The simulations were performed on a Beowulf cluster at the Informatikdienste of the University of Zürich, and we thank C. Bolliger and Dr. A. Godknecht for their help in setting up and maintaining the cluster. We thank A. Widmer (Novartis Pharma, Basel) for providing the molecular modeling program Witnotp, which was used for visual analysis of the trajectories. This work was supported by the Swiss National Science Foundation, the National Competence Center on Neural Plasticity and Repair, and KTI (Kommission Technologie und Innovation).

Received: May 25, 2005
Revised: June 20, 2005
Accepted: June 28, 2005
Published: October 11, 2005

References

Andreeva, N.S., and Rumsh, L.D. (2001). Analysis of crystal structures of aspartic proteinases: on the role of amino acid residues adjacent to the catalytic site of pepsin-like enzymes. Protein Sci. *10*, 2439–2450.

Andreeva, N., Dill, J., and Gilliland, G.L. (1992). Can enzymes adopt a self-inhibited form? results of X-ray crystallographic studies of chymosin. Biochem. Biophys. Res. Commun. *184*, 1074–1081.

Berman, H.M., Westbrook, J., Feng, Z., Gilliland, G., Bhat, T.N., Weissig, H., Shindyalov, I.N., and Bourne, P.E. (2000). The protein data bank. Nucleic Acids Res. *28*, 235–242.

Brooks, B.R., Bruccoleri, R.E., Olafson, B.D., States, D.T., Swaminathan, S., and Karplus, M. (1983). CHARMM – a program for macromolecular energy, minimization, and dynamics calculations. J. Comp. Chem. *4*, 187–217.

Cavasotto, C., and Abagyan, R. (2004). Protein flexibility in ligand docking and virtual screening to protein kinases. J. Mol. Biol. *337*, 209–225.

Caves, L.S., Evanseck, J.D., and Karplus, M. (1998). Locally accessible conformations of proteins: multiple molecular dynamics simulations of crambin. Protein Sci. *7*, 649–666.

Citron, M. (2004). β-secretase inhibition for the treatment of Alzheimer's disease–promise and challenge. Trends Pharmacol. Sci. *25*, 92–97.

Clemente, J.C., Moose, R.E., Hemrajani, R., Whitford, L.R., Govindasamy, L., Reutzel, R., McKenna, R., Agbandje-McKenna, M., Goodenow, M.M., and Dunn, B.M. (2004). Comparing the accumulation of active- and nonactive-site mutations in the HIV-1 protease. Biochemistry *43*, 12141–12151.

Coburn, C.A., Stachel, S.J., Li, Y.M., Rush, D.M., Steele, T.G., Chen-Dodson, E., Holloway, M.K., Xu, M., Huang, Q., Lai, M.T., et al. (2004). Identification of a small molecule nonpeptide active site β-secretase inhibitor that dislays a nontraditional binding mode for aspartyl proteases. J. Med. Chem. *47*, 6117–6119.

Collins, J.R., Burt, S.K., and Erickson, J.W. (1995). Flap opening in HIV-1 protease simulated by 'activated' molecular dynamics. Nat. Struct. Biol. *2*, 334–338.

Cumming, J.N., Iserloh, U., and Kennedy, M.E. (2004). Design and development of BACE-1 inhibitors. Curr. Opin. Drug Discov. Devel. *7*, 536–556.

Davies, D.R. (1990). The structure and function of the aspartic proteinases. Annu. Rev. Biophys. Biophys. Chem. *19*, 189–215.

Elber, R., and Karplus, M. (1990). Multiple conformational states of proteins: a molecular dynamics analysis of myoglobin. Science *235*, 318–321.

Essmann, U., Perera, L., Berkowitz, M.L., Darden, T., Lee, H., and Pedersen, L.G. (1995). A smooth particle mesh ewald method. J. Chem. Phys. *151*, 8577–8593.

Freedberg, D.I., Ishima, R., Jacob, J., Wang, Y.X., Kustanovich, I., Louis, J.M., and Torchia, D.A. (2002). Rapid structural fluctuations of the free HIV protease flaps in solution: relationship to crystal structures and comparison with predictions of dynamics calculations. Protein Sci. *11*, 221–232.

Ghosh, A.K., Hong, L., and Tang, J. (2002). β-secretase as a therapeutic target for inhibitor drugs. Curr. Med. Chem. *9*, 1135–1144.

Ghosh, A.K., Devasamudram, T., Hong, L., DeZutter, C., Xu, X., Weerasena, V., Koelsch, G., Bilcer, G., and Tang, J. (2005). Structure-based design of cycloamide-urethane-derived novel inhibitors of human brain memapsin 2 (β-secretase). Bioorg. Med. Chem. Lett. *15*, 15–20.

Gilliland, G.L., Winborne, E.L., Nachman, J., and Wlodawer, A. (1990). The three-dimensional structure of recombinant bovine chymosin at 2.3 Å resolution. Proteins *8*, 82–101.

Gorfe, A.A., Ferrara, P., Caflisch, A., Marti, D.N., Bosshard, H.R., and Jelesarov, I. (2002). Calculation of protein ionization equilibria with conformational sampling: pK(a) of a model leucine zipper, GCN4 and barnase. Proteins *46*, 41–60.

Grüninger-Leitch, F., Schlatter, D., Küng, E., Nobnlöck, P., and Döbeli, H. (2002). Substrate and inhibitor profile of BACE (β-secretase) and comparison with other mammalian aspartic proteases. J. Biol. Chem. *277*, 4687–4693.

Gustchina, A., Li, M., Phylip, L.H., Lees, W.E., Kay, J., and Wlodawer, A. (2002). An unusual orientation for Tyr75 in the active site of the aspartic proteinase from saccharomyces cerevisiae. Biochem. Biophys. Res. Commun. *295*, 1020–1026.

Gustchina, A., Li, M., Wunschmann, S., Chapman, M.D., Pomes, A., and Wlodawer, A. (2005). Crystal structure of cockroach allergen Bla g *2*, an unusual zinc binding aspartic protease with a novel mode of self-inhibition. J. Mol. Biol. *348*, 433–444.

Harte, W.E., Swaminathan, S., Mansuri, M.M., Martin, J.C., Rosenberg, I.E., and Beveridge, D.L. (1990). Domain communication in the dynamical structure of human immunodeficiency virus 1 protease. Proc. Natl. Acad. Sci. USA *87*, 8864–8868.

Harte, W.E., Swaminathan, S., and Beveridge, D.L. (1992). Molecular dynamics of HIV-1 protease. Proteins *13*, 175–194.

Hartigan, J.A. (1975). Clustering Algorithms (New York: Wiley).

Hong, L., and Tang, J. (2004). Flap position of free memapsin 2 (β-secretase), a model for flap opening in aspartic protease catalysis. Biochemistry *43*, 4689–4695.

Hong, L., Koelsch, G., Lin, X., Wu, S., Terzyan, S., Ghosh, A.K., Zhang, X.C., and Tang, J. (2000). Structure of the protease domain of memapsin 2 (β-secretase) complexed with inhibitor. Science *290*, 150–153.

Hong, L., Turner, R.T., Koelsch, G., Shin, D., Ghosh, A.K., and Tang, J. (2002). Crystal structure of memapsin 2 (β-secretase) in complex with an inhibitor OM00–3. Biochemistry *41*, 10963–10967.

Hoover, W.G. (1985). Canonical dynamics: equilibrium phase-space distributions. Phys. Rev. A. *31*, 1695–1697.

Huang, D., and Caflisch, A. (2004). Efficient evaluation of binding free energy using continuum electrostatic solvation. J. Med. Chem. *47*, 5791–5797.

Huang, D., Lüthi, U., Kolb, P., Edler, K., Cecchini, M., Audetat, S., Barberis, A., and Caflisch, A. (2005). Discovery of cell-permeable nonpeptide inhibitors of β-secretase by high-throughput docking and continuum electrostatics calculations. J. Med. Chem. *48*, 5108–5111.

Humphrey, W., Dalke, A., and Schulten, K. (1996). VMD - visual molecular dynamics. J. Mol. Graph. *14*, 33–38.

Ishima, R., Freedberg, D.I., Wang, Y.X., Louis, J.M., and Torchia, D.A. (1999). Flap opening and dimer-interface flexibility in the free and inhibitor-bound HIV protease, and their implications for function. Struct. Fold. Des. *7*, 1047–1055.

Kalé, L., Skeel, R., Bhandarkar, M., Brunner, R., Gursoy, A., Krawetz, N., Phillips, J., Shinozaki, A., Varadarajan, K., and Schulten, K.

(1999). NAMD2: greater scalability for parallel molecular dynamics. J. Comput. Phys. *151*, 283–312.

Katoh, E., Louis, J.M., Yamazaki, T., Gronenborn, A.M., Torchia, D.A., and Ishima, R. (2003). A solution NMR study of the binding kinetics and the internal dynamics of an HIV-1 protease-substrate complex. Protein Sci. *12*, 1376–1385.

Kovalskyy, D., Dubyna, V., Mark, A.E., and Kornelyuk, A. (2004). A molecular dynamics study of the structural stability of HIV-1 protease under physiological conditions: the role of Na+ ions in stabilizing the active site. Proteins *58*, 450–458.

Lee, A.Y., Gulnik, S.V., and Erickson, J.W. (1998). Conformational switching in an aspartic proteinase. Nat. Struct. Biol. *5*, 866–871.

Levy, Y., and Caflisch, A. (2003). Flexibility of monomeric and dimeric HIV-1 protease. J. Phys. Chem. B *107*, 3068–3079.

Levy, Y., Caflisch, A., Onuchic, J.N., and Wolynes, P.G. (2004). The folding and dimerization of HIV-1 protease: evidence for a stable monomer from simulations. J. Mol. Biol. *340*, 67–79.

MacKerell, A.D., Bashford, D., Bellott, M., Dunbrack, R.L., Evanseck, J.D., Field, M., Fischer, S., Gao, J., Kuchnir, L., Guo, L., et al. (1998). All-atom empirical potential for molecular modeling and dynamics studies of proteins. J. Phys. Chem. B *102*, 3586–3616.

Marcinkeviciene, J., Kopcho, L.M., Yang, T., Copeland, R.A., Glass, B.M., Combs, A.P., Falahatpisheh, N., and Thompson, L. (2002). Novel inhibition of porcine pepsin by a substituted piperidine. Preference for one of the enzyme conformers. J. Biol. Chem. *277*, 28677–28682.

Meagher, K.L., and Carlson, H.A. (2004). Incorporating protein flexibility in structure-based drug discovery: using HIV-1 protease as a test case. J. Am. Chem. Soc. *126*, 13276–13281.

Meagher, K.L., and Carlson, H.A. (2005). Solvation influences flap collapse in HIV-1 protease. Proteins *58*, 119–125.

Navia, M.A., Fitzgerald, P.M., McKeever, B.M., Leu, C.T., Heimbach, J.C., Herber, W.K., Sigal, I.S., Darke, P.L., and Springer, J.P. (1989). Three-dimensional structure of aspartyl protease from human immunodeficiency virus HIV-1. Nature *337*, 615–620.

Newman, M., Safro, M., Frazao, C., Khan, G., Zdanov, A., Tickle, I., Blundell, T., and Andreeva, N. (1991). X-ray analyses of aspartic proteinases. IV. Structure and refinement at 2.2Å resolution of bovine chymosin. J. Mol. Biol. *221*, 1295–1309.

Oefner, C., Binggeli, A., Breu, V., Bur, D., Clozel, J.P., D'Arcy, A., Dorn, A., Fischli, W., Grüninger, F., Guller, R., et al. (1999). Renin inhibition by substituted piperidines: a novel paradigm for the inhibition of monomeric aspartic proteinases? Chem. Biol. *6*, 127–131.

Park, H., and Lee, S. (2003). Determination of the active site protonation state of β-secretase from molecular dynamics simulation and docking experiment: implications for structure-based inhibitor design. J. Am. Chem. Soc. *125*, 16416–16422.

Patel, S., Vuillard, L., Cleasby, A., Murray, C.W., and Yon, J. (2004). Apo and inhibitor complex structures of BACE (β-secretase). J. Mol. Biol. *343*, 407–416.

Perryman, A.L., Lin, J.H., and McCammon, J.A. (2004). HIV-1 protease molecular dynamics of a wild-type and of the V82F/I84V mutant: possible contributions to drug resistance and a potential new target site for drugs. Protein Sci. *13*, 1108–1123.

Prasad, B.V., and Suguna, K. (2002). Role of water molecules in the structure and function of aspartic proteinases. Acta Crystallogr. D Biol. Crystallogr. *58*, 250–259.

Rahuel, J., Rasetti, V., Maibaum, J., Rueger, H., Goschke, R., Cohen, N.C., Stutz, S., Cumin, F., Fuhrer, W., Wood, J., and Grütter, M.G. (2000). Structure-based drug design: the discovery of novel nonpeptide orally active inhibitors of human renin. Chem. Biol. *7*, 493–504.

Rajamani, R., and Reynolds, C.H. (2004). Modeling the protonation states of the catalytic aspartates in β-secretase. J. Med. Chem. *47*, 5159–5166.

Roggo, S. (2002). Inhibition of BACE, a promising approach to Alzheimer's disease therapy. Curr. Top. Med. Chem. *2*, 359–370.

Šali, A., Veerapandian, B., Cooper, J.B., Moss, D.S., Hofmann, T., and Blundell, T.L. (1992). Domain flexibility in aspartic proteinase. Proteins *12*, 158–170.

Settanni, G., Rao, F., and Caflisch, A. (2005). Φ-value analysis by molecular dynamics simulations of reversible folding. Proc. Natl. Acad. Sci. USA *102*, 628–633.

Stachel, S.J., Coburn, C.A., Steele, T.G., Jones, K.G., Loutzenhiser, E.F., Gregro, A.R., Rajapakse, H.A., Lai, M.T., Crouthamel, M.C., Xu, M., et al. (2004). Structure-based design of potent and selective cell-permeable inhibitors of human β-secretase (BACE-1). J. Med. Chem. *47*, 6447–6450.

Strop, P., Sedlacek, J., Stys, J., Kaderabkova, Z., Blaha, I., Pavlickova, L., Pohl, J., Fabry, M., Kostka, V., Newman, M., et al. (1990). Engineering enzyme subsite specificity: preparation, kinetic characterization, and X-ray analysis at 2.0-Å resolution of Val111Phe site-mutated calf chymosin. Biochemistry *29*, 9863–9871.

Suguna, K., Padlan, E.A., Smith, C.W., Carlson, W.D., and Davies, D.R. (1987). Binding of a reduced peptide inhibitor to the aspartic proteinase from rhizopus chinensis: implications for a mechanism of action. Proc. Natl. Acad. Sci. USA *84*, 7009–7013.

Tang, J., and Koelsch, G. (1995). A possible function of a flap of aspartic proeases: the capture of substrate side chains determines the specificity of cleavage positions. Peptide Lett. *2*, 257–266.

Teague, S.J. (2003). Implications of protein flexibility for drug discovery. Nat. Rev. Drug Discov. *2*, 527–541.

Toulokhonova, L., Metzler, W.J., Witmer, M.R., Copeland, R.A., and Marcinkeviciene, J. (2003). Kinetic studies on β-site amyloid precursor protein-cleaving enzyme (BACE). Confirmation of an iso mechanism. J. Biol. Chem. *278*, 4582–4589.

Turner, R.T., Hong, L., Koelsch, G., Ghosh, A.K., and Tang, J. (2005). Structural locations and functional roles of new subsites S5, S6, and S7 in memapsin 2 (β-secretase). Biochemistry *44*, 105–112.

Vassar, R., Bennett, B.D., Babu-Khan, S., Kahn, S., Mendiaz, E.A., Denis, P., Teplow, D.B., Ross, S., Amarante, P., Loeloff, R., et al. (1999). Beta-secretase cleavage of Alzheimer's amyloid precursor protein by the transmembrane aspartic protease BACE. Science *286*, 735–741.

Wittayanarakul, K., Aruksakunwong, O., Saen-Oon, S., Chantratita, W., Parasuk, V., Sompornpisut, P., and Hannongbua, S. (2005). Insights into saquinavir resistance in the G48V HIV-1 protease: quantum calculations and molecular dynamics simulations. Biophys. J. *88*, 867–879.

Wlodawer, A., and Gustchina, A. (2000). Structural and biochemical studies of retroviral proteases. Biochim. Biophys. Acta *1477*, 16–34.

Wlodawer, A., Miller, M., Jaskolski, M., Sathyanarayana, B.K., Baldwin, E., Weber, I.T., Selk, L.M., Clawson, L., Schneider, J., and Kent, S.B. (1989). Conserved folding in retroviral proteases: crystal structure of a synthetic HIV-1 protease. Science *245*, 616–621.

Wood, J.M., Maibaum, J., Rahuel, J., Grütter, M.G., Cohen, N.C., Rasetti, V., Ruger, H., Goschke, R., Stutz, S., Fuhrer, W., et al. (2003). Structure-based design of aliskiren, a novel orally effective renin inhibitor. Biochem. Biophys. Res. Commun. *308*, 698–705.

Zhu, Z., Schuster, D.I., and Tuckerman, M.E. (2003). Molecular dynamics study of the connection between flap closing and binding of fullerene-based inhibitors of the HIV-1 protease. Biochemistry *42*, 1326–1333.

Zoete, V., Michielin, O., and Karplus, M. (2002). Relation between sequence and structure of HIV-1 protease inhibitory: a model system for the analysis of protein flexibility. J. Mol. Biol. *315*, 21–52.